MICROSCOPIC INTERLAMINAR ANALYSIS OF CROSS-PLY LAMINATES USING HOMOGENIZATION THEORY

Tetsuya Matsuda*, Dai Okumura, Nobutada Ohno**, Masamichi Kawai***
****Department of Engineering Mechanics and Energy, University of Tsukuba**
****Department of Mechanical Science and Engineering, Nagoya University**

Keywords: *Interlaminar, Long fiber-reinforced laminate, Homogenization, Point-symmetry*

Abstract

In this study, a method for the three-dimensional microscopic interlaminar analysis of cross-ply laminates is developed based on a homogenization theory in order to analyze the microscopic interaction between unidirectional long fiber-reinforced laminae. A unit cell of a cross-ply laminate, which includes interlaminar areas, is defined under the assumption that each lamina in the laminate has a transversely square fiber array. Then, showing that the laminate has a point-symmetric internal structure, the symmetry is utilized to introduce a half of the unit cell as the domain of analysis. Moreover, the domain of analysis is divided into substructures using the substructure method. The present method is then applied to the analysis of interlaminar stress distributions in a carbon fiber/epoxy cross-ply laminate under an in-plane off-axis tensile load. It is thus shown that a marked microscopic shear stress occurs at the interface between the 0˚- and 90˚-plies.

1 Introduction

Long fiber-reinforced laminates are important engineering materials because of their high specific stiffness, high specific strength, and many other advantageous features. Since the laminates are generally manufactured by stacking unidirectional long fiber-reinforced laminae, the laminates have interfaces between the laminae, i.e., interlaminar areas. In these areas, microscopic failures, e.g., matrix cracking, delamination and so forth, are apt to occur. Such microscopic failures can result in the macroscopic failure of laminates. Thus, it is indispensable to analyze the microscopic stress/strain distributions at interlaminar areas.

The microscopic interlaminar analysis mentioned above is different from the macroscopic interlaminar analysis in which the laminae are regarded as homogeneous materials. In microscopic interlaminar analysis, laminae are not considered homogeneous but heterogeneous materials that have microscopic internal structures comprised of fibers and matrices. This analysis provides detailed stress/strain distributions at interlaminar areas microscopically. In addition, the analysis elucidates how far the influence of interaction between laminae reaches from interfaces between laminae on a microscopic level. At areas outside the effective range of the microscopic interaction between laminae, it may be possible to treat the laminae as homogeneous materials instead of heterogeneous materials. It is therefore of significance to perform the microscopic interlaminar analysis.

Finite element method (FEM) based analysis is one of the most useful approaches for microscopic interlaminar analysis, because FEM is capable of modeling the microstructures of laminae explicitly and in detail. The pioneering work of Pagano and Rybicki [1] has analyzed the microscopic interlaminar stress distributions in a unidirectional long fiber-reinforced composite with a free-edge. Recently, Raghavan et al. [2], Ghosh et al. [3] and Raghavan and Ghosh [4] have had great success in finding the interlaminar stress distributions in unidirectional composites microscopically using the Voronoi cell FEM [5] in conjunction with the adaptive mesh method [6]. These studies, however, dealt only with a two-dimensional or a generalized two-dimensional analysis of unidirectional long fiber-reinforced composites. The present authors have more interest in the interlaminar analysis of multidirectional fiber-reinforced laminates, in which the microscopic interlaminar stress/strain must be analyzed three-dimensionally.

In the previous papers [7,8], we analyzed the in-plane elastic-viscoplastic behavior of multidirectional CFRP laminates using the homogenization theory of nonlinear time-dependent composites [9,10] combined with the classical

lamination theory. The homogenization theory is based on the unit cell problem [11-13], and enables us to analyze not only the macroscopic properties of composites, but also the microscopic distributions of stress and strain in unit cells. The analysis procedure in the previous papers was as follows: First, a unit cell which contains fibers and matrix as a microstructure of each lamina was defined and the microscopic distributions of stress and strain rates in each lamina were calculated by the homogenization theory. Next, the microscopic stress and strain rates with respect to the unit cell were averaged, obtaining the macroscopic stress and strain rates of each lamina. Finally, using the macroscopic stress and strain rates of the laminae, the macroscopic constitutive relation of a laminate was derived based on the classical lamination theory. This method, therefore, was able to analyze the microscopic stress/strain distributions at internal areas of laminae, but not able to analyze those at interlaminar areas.

However, we can perform microscopic interlaminar analysis of laminates using the homogenization theory by assuming the microscopic internal structure of a laminate as illustrated in Fig. 1, and by defining a unit cell of the laminate. The use of such a unit cell allows us to analyze the microscopic stress/strain distributions in the laminate three-dimensionally, as well as the macroscopic behavior of the laminate. Employing this method, therefore, not only the microscopic interlaminar stress/strain distributions, but also the effective range of microscopic interaction between laminae can be investigated.

In this study, a novel method for the three-dimensional microscopic interlaminar analysis of cross-ply laminates is proposed based on the homogenization theory. Utilizing the point-symmetry of the internal structure in the laminate, the domain of analysis is reduced by half based on our previous result [14]. The substructure method [15] is subsequently introduced into the homogenization theory to reduce computational efforts further. The proposed method is then applied to the analysis of microscopic stress distributions at an interlaminar area in a carbon fiber/epoxy cross-ply laminate subjected to an in-plane off-axis tensile load. Finally, the microscopic influence of interaction between laminae in the interlaminar area is discussed.

2 Three-Dimensional Microscopic Interlaminar Analysis of Cross-Ply Laminate

In the present study, we consider a cross-ply laminate illustrated in Fig. 1, in which each unidirectional long fiber-reinforced lamina is assumed to have a square fiber array and possessing $2N$ fibers in the stacking direction (y_1-direction). The laminate is subjected to an in-plane uniaxial tensile load with an off-axis angle θ as shown in Fig. 1, and exhibits macroscopically uniform elastic deformation. The deformation is assumed to be infinitesimal.

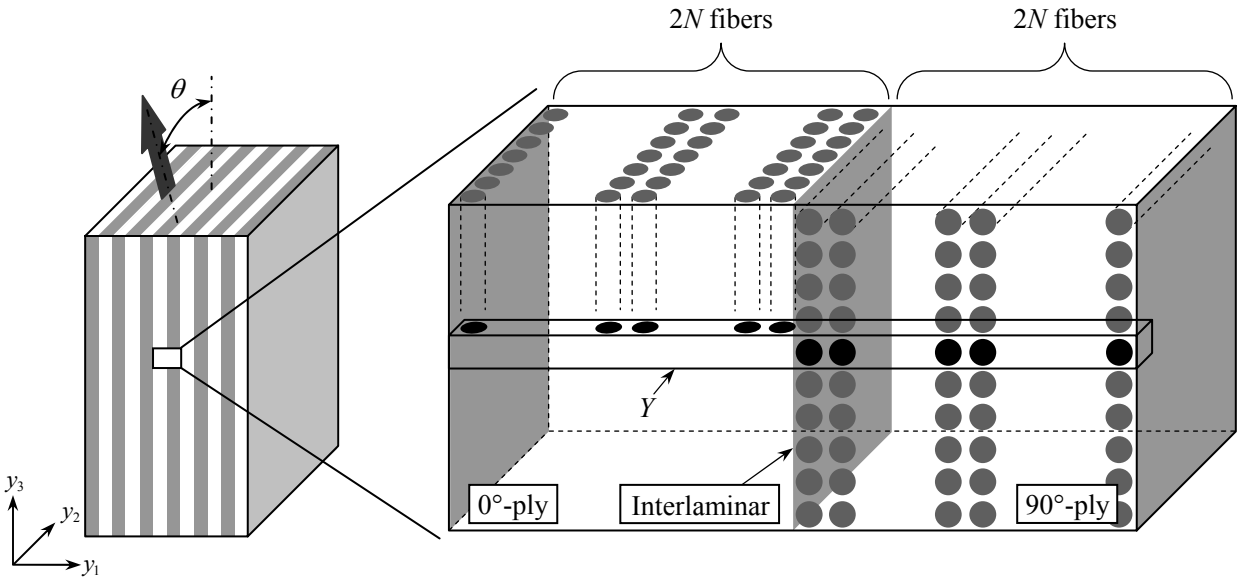

Fig. 1. Microscopic internal structure and unit cell Y of cross-ply laminate subjected to in-plane off-axis tensile load.

2.1 Homogenization Theory

In order to apply the homogenization theory based on the unit cell problem [11-13] to the present analysis, we first define a unit cell Y of the laminate as shown in Fig. 1 so that Y includes the interfaces between laminae. The constituents of Y, i.e., fibers and matrix, are assumed to be elastic materials, and obey the following constitutive equation:

$$\sigma_{ij} = c_{ijkl}\varepsilon_{kl}\,, \tag{1}$$

where σ_{ij} and ε_{kl} denote the microscopic stress and strain, respectively, and c_{ijkl} signifies the elastic stiffness satisfying $c_{ijkl} = c_{jikl} = c_{ijlk} = c_{klij}$. The homogenization theory then gives the relation between macroscopic stress Σ_{ij} and macroscopic strain E_{ij} , and the microscopic stress σ_{ij} :

$$\Sigma_{ij} = \left\langle c_{ijpq}(\delta_{pk}\delta_{ql} + \chi^{kl}_{p,q})\right\rangle E_{kl}\,, \tag{2}$$

$$\sigma_{ij} = c_{ijpq}(\delta_{pk}\delta_{ql} + \chi^{kl}_{p,q})E_{kl}\,, \tag{3}$$

where $(\,)_{,i}$ stands for the differentiation with respect to y_i, δ_{ij} indicates Kronecker's delta, and $\langle\ \rangle$ designates the volume average with respect to Y defined as $\langle \# \rangle = |Y|^{-1}\int_Y \# dY$, in which $|Y|$ signifies the volume of Y. Moreover, χ^{kl}_i in Eqs. 2 and 3 denotes the characteristic function obtained by solving the following boundary value problem with the Y-periodic boundary condition:

$$\int_Y c_{ijpq}\chi^{kl}_{p,q} v_{i,j} dY = -\int_Y c_{ijkl} v_{i,j} dY\,, \tag{4}$$

where v_i is an arbitrary field of perturbed displacement satisfying the Y-periodicity. Since the above problem Eq. 4 is generally solved by FEM, we rewrite Eq. 4 in the finite element discretized form:

$$\boldsymbol{K}\boldsymbol{\chi}^{kl} = \boldsymbol{F}^{kl},\ (kl = 11, 22, \ldots, 31)\,, \tag{5}$$

where $\boldsymbol{\chi}^{kl}$ denotes the nodal vector of χ^{kl}_i , and $\boldsymbol{K}$ and $\boldsymbol{F}^{kl}$ are expressed as

$$\boldsymbol{K} = \int_Y \boldsymbol{B}^{\mathrm{T}}\boldsymbol{C}\boldsymbol{B} dY\,,\ \boldsymbol{F}^{kl} = -\int_Y \boldsymbol{B}^{\mathrm{T}}\boldsymbol{C}^{kl} dY\,. \tag{6}$$

Here, $\boldsymbol{B}$ denotes the transformation matrix from nodal displacement to strain, $\boldsymbol{C}$ is the elastic stiffness matrix representing c_{ijkl} , T stands for the transpose, and $\boldsymbol{C}^{kl} = \{c_{11kl}\ \ c_{22kl}\ \ c_{33kl}\ \ c_{12kl}\ \ c_{23kl}\ \ c_{31kl}\}^{\mathrm{T}}$.

By solving Eq. 5 and finding $\boldsymbol{\chi}^{kl}$, the macroscopic elastic behavior of the laminate can be analyzed using Eq. 2 and the microscopic stress at any point in Y can be determined based on Eq. 3. Adopting the present framework of analysis, therefore, both the microscopic interlaminar stress distribution and the effective range of microscopic interaction between 0°- and 90°-plies can be investigated under macroscopic load.

2.2 Semiunit Cell

In the previous section, the framework of microscopic interlaminar analysis of cross-ply laminates was described based on the homogenization theory. The analysis, however, entails a huge amount of computational resources because of the large size of $\boldsymbol{K}$ in Eq. 5, which is due to employing the large-scale unit cell containing a lot of fibers and matrix. Thus, in this section, the domain of analysis is reduced by half utilizing the point-symmetry of internal structure of the laminate.

Let us consider a half of the unit cell as shown in Fig. 2, which will be referred to as a semiunit cell $\tilde{Y}$ hereafter. A close look at Fig. 2 then reveals that the internal structure of the laminate has a point-symmetry with respect to the centers of left and right lateral boundary facets of $\tilde{Y}$, C_A and C_B . As a consequence, the distribution of χ^{kl}_i also satisfies the point-symmetry with respect to these points. Using the point-symmetry as a boundary condition on the left and right lateral boundary facets of $\tilde{Y}$, we are able to employ $\tilde{Y}$ instead of Y as the domain of analysis, leading to the following boundary value problem with respect to $\tilde{Y}$ [14]:

$$\int_{\tilde{Y}} c_{ijpq}\chi^{kl}_{p,q} v_{i,j} d\tilde{Y} = -\int_{\tilde{Y}} c_{ijkl} v_{i,j} d\tilde{Y}\,. \tag{7}$$

Since the above boundary value problem Eq. 7 has the same form as Eq. 4, the problem can be solved in the same manner using FEM as in Eq. 4. Thus, Eq. 7 is rewritten into the finite element discretized form:

$$\tilde{\boldsymbol{K}}\boldsymbol{\chi}^{kl} = \tilde{\boldsymbol{F}}^{kl},\ (kl = 11, 22, \ldots, 31)\,, \tag{8}$$

where $\tilde{\boldsymbol{K}}$ and $\tilde{\boldsymbol{F}}^{kl}$ are expressed as follows:

$$\tilde{\boldsymbol{K}} = \int_{\tilde{Y}} \boldsymbol{B}^{\mathrm{T}}\boldsymbol{C}\boldsymbol{B} d\tilde{Y}\,,\ \tilde{\boldsymbol{F}}^{kl} = -\int_{\tilde{Y}} \boldsymbol{B}^{\mathrm{T}}\boldsymbol{C}^{kl} d\tilde{Y}\,. \tag{9}$$

It is noted that, when solving Eq. 8, not the Y-periodic but the point-symmetric boundary condition with respect to C_A and C_B is imposed on $\boldsymbol{\chi}^{kl}$, on the left and right lateral boundary facets of $\tilde{Y}$. Whereas, on the other boundary facets of $\tilde{Y}$, the Y-periodic boundary condition is imposed on $\boldsymbol{\chi}^{kl}$.

It is emphasized that that the use of the semiunit cell $\tilde{Y}$ reduces the degrees of freedom (the number of nodes) in the boundary value problem

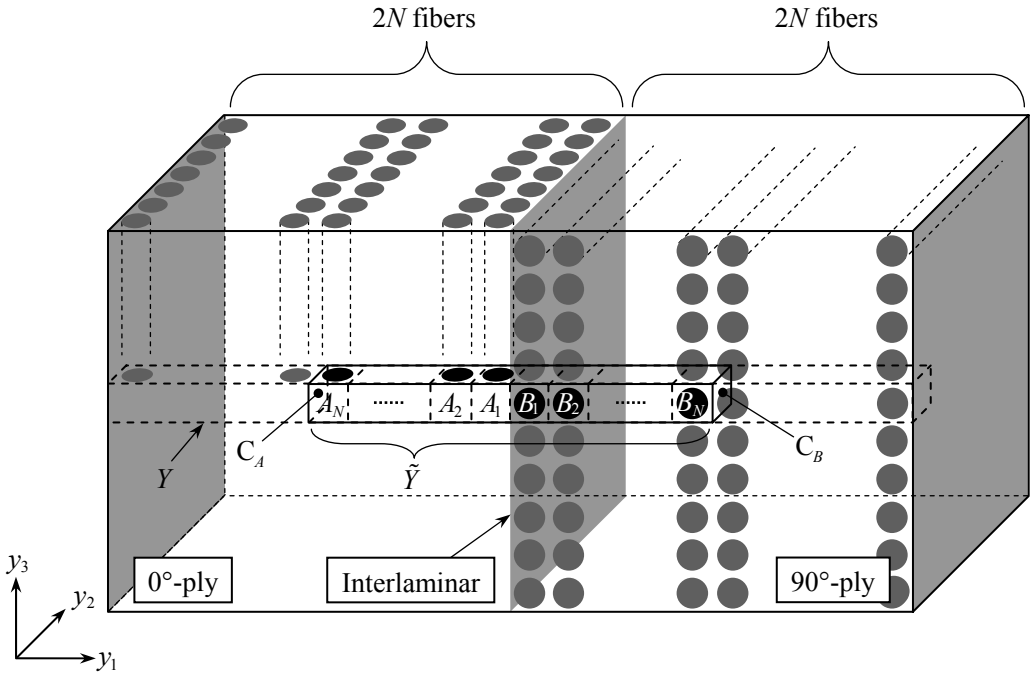

Fig. 2. Semiunit cell $\tilde{Y}$ and point symmetric internal structure of laminate with respect to centers of left and right lateral boundary facets of $\tilde{Y}$, C_A and C_B.

almost by half, compared with the analysis using the whole unit cell Y mentioned in the previous section. This yields a considerable reduction in computational load.

2.3 Substructure Method

In the previous section, the semiunit cell $\tilde{Y}$ was introduced so that we could reduce the domain of analysis by half. But, even $\tilde{Y}$ is still considerably large-scale for computation. In this section, therefore, the substructure method [15] is introduced into the homogenization theory to solve the boundary value problem Eq. 8.

First, note that the semiunit cell $\tilde{Y}$ consists of cubic cells A_i $(i=1,2,\ldots,N)$ and B_i $(i=1,2,\ldots,N)$ for the 0°- and 90°-plies, respectively, as shown in Fig. 2. Hence, we divide $\tilde{Y}$ into A_i and B_i as substructures, and then derive the boundary value problems for the substructures in finite element discretized form as follows:

$$\boldsymbol{K}_A \boldsymbol{\chi}_{A_i}^{kl} = \boldsymbol{F}_A^{kl},\ (i=1,2,\ldots,N), \qquad (10)$$

$$\boldsymbol{K}_B \boldsymbol{\chi}_{B_i}^{kl} = \boldsymbol{F}_B^{kl},\ (i=1,2,\ldots,N), \qquad (11)$$

where $\boldsymbol{\chi}_{A_i}^{kl}$ and $\boldsymbol{\chi}_{B_i}^{kl}$ denote the nodal vectors of characteristic function in A_i and B_i, respectively, and $\boldsymbol{K}_A$, $\boldsymbol{F}_A^{kl}$, $\boldsymbol{K}_B$ and $\boldsymbol{F}_B^{kl}$ have the following expressions:

$$\boldsymbol{K}_A = \int_{A_i} \boldsymbol{B}^{\mathrm{T}} \boldsymbol{C} \boldsymbol{B} dA_i,\ \boldsymbol{F}_A^{kl} = -\int_{A_i} \boldsymbol{B}^{\mathrm{T}} \boldsymbol{C}^{kl} dA_i, \qquad (12)$$

$$\boldsymbol{K}_B = \int_{B_i} \boldsymbol{B}^{\mathrm{T}} \boldsymbol{C} \boldsymbol{B} dB_i,\ \boldsymbol{F}_B^{kl} = -\int_{B_i} \boldsymbol{B}^{\mathrm{T}} \boldsymbol{C}^{kl} dB_i. \qquad (13)$$

It is noteworthy that all A_i have the common $\boldsymbol{K}_A$ and $\boldsymbol{F}_A^{kl}$ because the geometry and material properties of all A_i are the same. For the same reason, all B_i have the common $\boldsymbol{K}_B$ and $\boldsymbol{F}_B^{kl}$, which are easily obtained by rotating A_i by 90° with respect to y_1-axis. It is therefore enough for us to calculate $\boldsymbol{K}_A$, $\boldsymbol{F}_A^{kl}$, $\boldsymbol{K}_B$ and $\boldsymbol{F}_B^{kl}$ only once.

Next, the components of $\boldsymbol{\chi}_{A_i}^{kl}$ are divided into two parts, $\boldsymbol{\chi}_{A_i}^{kl(\Omega)}$ and $\boldsymbol{\chi}_{A_i}^{kl(\Gamma)}$, which represent the characteristic functions at the internal and the boundary nodes, respectively. The components of $\boldsymbol{\chi}_{B_i}^{kl}$ are also divided into $\boldsymbol{\chi}_{B_i}^{kl(\Omega)}$ and $\boldsymbol{\chi}_{B_i}^{kl(\Gamma)}$. Then, the boundary value problems for A_i and B_i, Eqs. 10 and 11, are rewritten into the following equations, respectively:

$$\begin{bmatrix} \boldsymbol{K}_A^{(\Omega)} & \boldsymbol{K}_A^{(\Omega\Gamma)} \\ \boldsymbol{K}_A^{(\Gamma\Omega)} & \boldsymbol{K}_A^{(\Gamma)} \end{bmatrix} \begin{Bmatrix} \boldsymbol{\chi}_{A_i}^{kl(\Omega)} \\ \boldsymbol{\chi}_{A_i}^{kl(\Gamma)} \end{Bmatrix} = \begin{Bmatrix} \boldsymbol{F}_A^{kl(\Omega)} \\ \boldsymbol{F}_A^{kl(\Gamma)} \end{Bmatrix}, \qquad (14)$$

$$\begin{bmatrix} \boldsymbol{K}_B^{(\Omega)} & \boldsymbol{K}_B^{(\Omega\Gamma)} \\ \boldsymbol{K}_B^{(\Gamma\Omega)} & \boldsymbol{K}_B^{(\Gamma)} \end{bmatrix} \begin{Bmatrix} \boldsymbol{\chi}_{B_i}^{kl(\Omega)} \\ \boldsymbol{\chi}_{B_i}^{kl(\Gamma)} \end{Bmatrix} = \begin{Bmatrix} \boldsymbol{F}_B^{kl(\Omega)} \\ \boldsymbol{F}_B^{kl(\Gamma)} \end{Bmatrix}, \quad (15)$$

and we obtain

$$\boldsymbol{\chi}_{A_i}^{kl(\Omega)} = \left(\boldsymbol{K}_A^{(\Omega)}\right)^{-1} \left(\boldsymbol{F}_A^{kl(\Omega)} - \boldsymbol{K}_A^{(\Omega\Gamma)} \boldsymbol{\chi}_{A_i}^{kl(\Gamma)}\right), \quad (16)$$

$$\boldsymbol{\chi}_{B_i}^{kl(\Omega)} = \left(\boldsymbol{K}_B^{(\Omega)}\right)^{-1} \left(\boldsymbol{F}_B^{kl(\Omega)} - \boldsymbol{K}_B^{(\Omega\Gamma)} \boldsymbol{\chi}_{B_i}^{kl(\Gamma)}\right). \quad (17)$$

The elimination of $\boldsymbol{\chi}_{A_i}^{kl(\Omega)}$ and $\boldsymbol{\chi}_{B_i}^{kl(\Omega)}$ from Eqs. 14 and 15 using the above equations, respectively, yields

$$\bar{\boldsymbol{K}}_A^{(\Gamma)} \boldsymbol{\chi}_{A_i}^{kl(\Gamma)} = \bar{\boldsymbol{F}}_A^{kl(\Gamma)}, \quad (18)$$

$$\bar{\boldsymbol{K}}_B^{(\Gamma)} \boldsymbol{\chi}_{B_i}^{kl(\Gamma)} = \bar{\boldsymbol{F}}_B^{kl(\Gamma)}, \quad (19)$$

where $\bar{\boldsymbol{K}}_A^{(\Gamma)}$, $\bar{\boldsymbol{F}}_A^{kl(\Gamma)}$, $\bar{\boldsymbol{K}}_B^{(\Gamma)}$ and $\bar{\boldsymbol{F}}_B^{kl(\Gamma)}$ are expressed as follows:

$$\begin{aligned} \bar{\boldsymbol{K}}_A^{(\Gamma)} &= \boldsymbol{K}_A^{(\Gamma)} - \boldsymbol{K}_A^{(\Gamma\Omega)} \left(\boldsymbol{K}_A^{(\Omega)}\right)^{-1} \boldsymbol{K}_A^{(\Omega\Gamma)}, \\ \bar{\boldsymbol{F}}_A^{kl(\Gamma)} &= \boldsymbol{F}_A^{kl(\Gamma)} - \boldsymbol{K}_A^{(\Gamma\Omega)} \left(\boldsymbol{K}_A^{(\Omega)}\right)^{-1} \boldsymbol{F}_A^{kl(\Omega)}, \end{aligned} \quad (20)$$

$$\begin{aligned} \bar{\boldsymbol{K}}_B^{(\Gamma)} &= \boldsymbol{K}_B^{(\Gamma)} - \boldsymbol{K}_B^{(\Gamma\Omega)} \left(\boldsymbol{K}_B^{(\Omega)}\right)^{-1} \boldsymbol{K}_B^{(\Omega\Gamma)}, \\ \bar{\boldsymbol{F}}_B^{kl(\Gamma)} &= \boldsymbol{F}_B^{kl(\Gamma)} - \boldsymbol{K}_B^{(\Gamma\Omega)} \left(\boldsymbol{K}_B^{(\Omega)}\right)^{-1} \boldsymbol{F}_B^{kl(\Omega)}. \end{aligned} \quad (21)$$

Finally, Eqs. 18 and 19 are assembled into one equation that is a boundary value problem with respect to only the boundary nodes of all substructures:

$$\boldsymbol{K}^{(\Gamma)} \boldsymbol{\chi}^{kl(\Gamma)} = \boldsymbol{F}^{kl(\Gamma)}, \quad (22)$$

where $\boldsymbol{K}^{(\Gamma)}$ stands for the matrix consisting of $\bar{\boldsymbol{K}}_A^{(\Gamma)}$ and $\bar{\boldsymbol{K}}_B^{(\Gamma)}$, $\boldsymbol{F}^{kl(\Gamma)}$ indicates the vector consisting of $\bar{\boldsymbol{F}}_A^{kl(\Gamma)}$ and $\bar{\boldsymbol{F}}_B^{kl(\Gamma)}$, and $\boldsymbol{\chi}^{kl(\Gamma)}$ denotes the nodal vector of characteristic function at the boundary nodes of substructures. The characteristic function $\boldsymbol{\chi}^{kl(\Gamma)}$ is determined by solving Eq. 22 with appropriate boundary conditions, i.e., the point-symmetric and the Y-periodic conditions stated in Section 2.2, and the continuity condition at the joint nodes of adjacent substructures. Then, the characteristic functions at the internal nodes, $\boldsymbol{\chi}_{A_i}^{kl(\Omega)}$ and $\boldsymbol{\chi}_{B_i}^{kl(\Omega)}$, are calculated using Eqs. 16 and 17.

In general, the total number of boundary nodes of all substructures is much less than the number of all nodes in the domain of analysis, resulting in a significant reduction of computational memory and time. Incidentally, Okumura et al. [16] applied the substructure method to an in-plane buckling analysis of hexagonal honeycombs using the homogenization theory of finite deformation [17].

3 Analysis

In this section, the present method is applied to the microscopic interlaminar analysis of a carbon fiber/epoxy cross-ply laminate under in-plane off-axis tensile load.

3.1 Cross-Ply Laminate and Macroscopic Boundary Condition

Considering that the carbon fiber/epoxy cross-ply laminate is made of general use prepreg sheets, each lamina is assumed to have 16 fibers in the stacking direction (N=8). The volume fraction of fibers is taken to be 56% as in the previous studies [7,8]. The laminate is subjected to the in-plane off-axis tensile load with an off-axis angle $\theta = 45°$. The macroscopic strain in the loading direction, E_θ, is prescribed to be 0.5%. The present analysis is performed under the macroscopic plane stress condition.

3.2 Substructures and Finite Element Discretization

As mentioned in Section 2.3, the semiunit cell $\tilde{Y}$ is divided into cubic substructures A_i (i=1,2,...,8) and B_i (i=1,2,...,8). Moreover, A_i and B_i are discretized into eight-node isoparametric elements as depicted in Fig. 3. Both the finite element meshes have 4320 elements and 5005 nodes, respectively.

If we employed the whole unit cell Y as the domain of analysis, we would be forced to solve the boundary value problem Eq. 5 with 464763 degrees of freedom because the unit cell Y would have 154921 nodes. By contrast, with the present method,

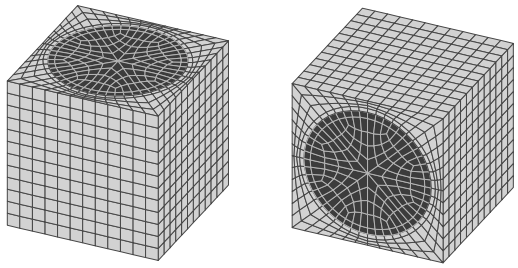

(a) (b)

Fig. 3. Substructures and finite element meshes; (a) A_i (0°-ply), (b) B_i (90°-ply).

the degrees of freedom in the boundary value problem Eq. 22 is only 62304 because the number of boundary nodes of each substructure is 1298. This reduction in degrees of freedom demonstrates the efficiency of the present method.

3.3 Material Properties

The carbon fibers are regarded as transversely isotropic elastic materials, while the epoxy matrix as an isotropic elastic material. The material constants used in the present analysis are listed in Table 1 [7,8]. In the Table, the subscripts L and T indicate the longitudinal and the transverse directions of fibers, respectively.

3.4 Results of Analysis

Figures 4(a)-(c) show the vector distributions of resultant shear stress $[(\sigma_{12})^2+(\sigma_{13})^2]^{1/2}$ at three parts in the laminate, i.e., the midsection of 0°-ply (left lateral surface of A_8) [Fig. 4(a)], the vicinity of the interlaminar plane (interface between A_1 and A_2) [Fig. 4(b)], and the interlaminar plane (interface between A_1 and B_1) [Fig. 4(c)]. In the figures, only the stress distributions in 0°-ply are depicted because the stress distributions in the 0°- and 90°-plies are symmetrical. First, as seen in Fig. 4(c), a considerably high shear stress occurs at the interlaminar plane microscopically. This is caused by the rotation of fibers in the 0°- and 90°-plies toward the loading direction. The maximum resultant shear stress is about 9 MPa, which reaches 21% of the macroscopic tensile stress (73 MPa) in terms of von Mises equivalent stress. By contrast, such a shear stress disappears in the vicinity of the interlaminar plane as shown in Fig. 5(b). In addition, no shear stress occurs at the midsection of 0°-ply [Fig. 4(a)]. These results suggest that the microscopic interaction between 0°- and 90°-plies is considerably local.

Next, the distributions of out-of-plane normal stress σ_{11} are shown in Figs. 5 (a)-(c). These figures indicate that the out-of-plane tensile and compressive stresses take place in the laminate microscopically, although the laminate is subjected to only an in-plane tensile load macroscopically. The interlaminar normal stress is lower than the interlaminar shear stress, but the same tendency is observed, i.e. the stress distribution at the interlaminar plane is markedly different from those at the other two parts. As illustrated in Fig. 5(c), at the interlaminar plane, the tensile and compressive stresses occur along the $\theta=45°$ and the $\theta=-45°$ directions, respectively, which seems to be caused by the rotation of fibers in 0°- and 90°-plies toward the loading direction. By contrast, in the vicinity of the interlaminar plane, σ_{11} distributes uniformly with respect to the y_3-axis as shown in Fig. 5(b). This distribution of σ_{11} is almost the same as that at the midsection of the 0°-ply [Fig. 5(a)], showing the local interaction of the two plies. Incidentally, we also analyzed microscopic stress distributions with on-axis tensile loading, i.e., at $\theta=0°$. The results exhibited the same tendency as the results of $\theta=45°$ described above.

Let us emphasize that such microscopic interlaminar stress distributions as discussed in this section can be found only by means of the microscopic analysis which explicitly takes into account microstructures in laminae.

Table 1. Material constants [7,8].

Carbon fiber	$E_{LL}=240$ [GPa]	$\nu_{TT}=0.49$
	$E_{TT}=15.5$ [GPa]	$\nu_{LT}=0.28$
	$G_{LT}=24.7$ [GPa]	
Epoxy	$E=3.5$ [GPa]	$\nu=0.35$

4 Conclusions

In this study, the distributions of microscopic interlaminar stress in a CFRP cross-ply laminate subjected to an in-plane off-axis tensile load were analyzed three-dimensionally using a newly proposed method based on the homogenization theory. In the proposed method, the domain of analysis was reduced by half using the point-symmetry of internal structure of laminate, resulting in marked reduction of computational efforts. In addition, the substructure method was introduced into the homogenization theory, which further increased computational efficiency. The analysis results showed that the maximum value of interlaminar resultant shear stress reached more than 20% of the macroscopic tensile stress applied to the laminate in terms of von Mises equivalent stress. In contrast, such microscopic shear stress disappeared at a distance of about a fiber diameter away from the interface between the 0°- and 90°-plies, indicating that the microscopic interaction between the two plies was considerably local. It therefore can be said that it is necessary to consider the microscopic structure consisting of fibers and matrix around the interface of laminae, while the microscopic structure at a distance of more than a fiber diameter away from the interface may be replaced by the equivalent homogeneous material.

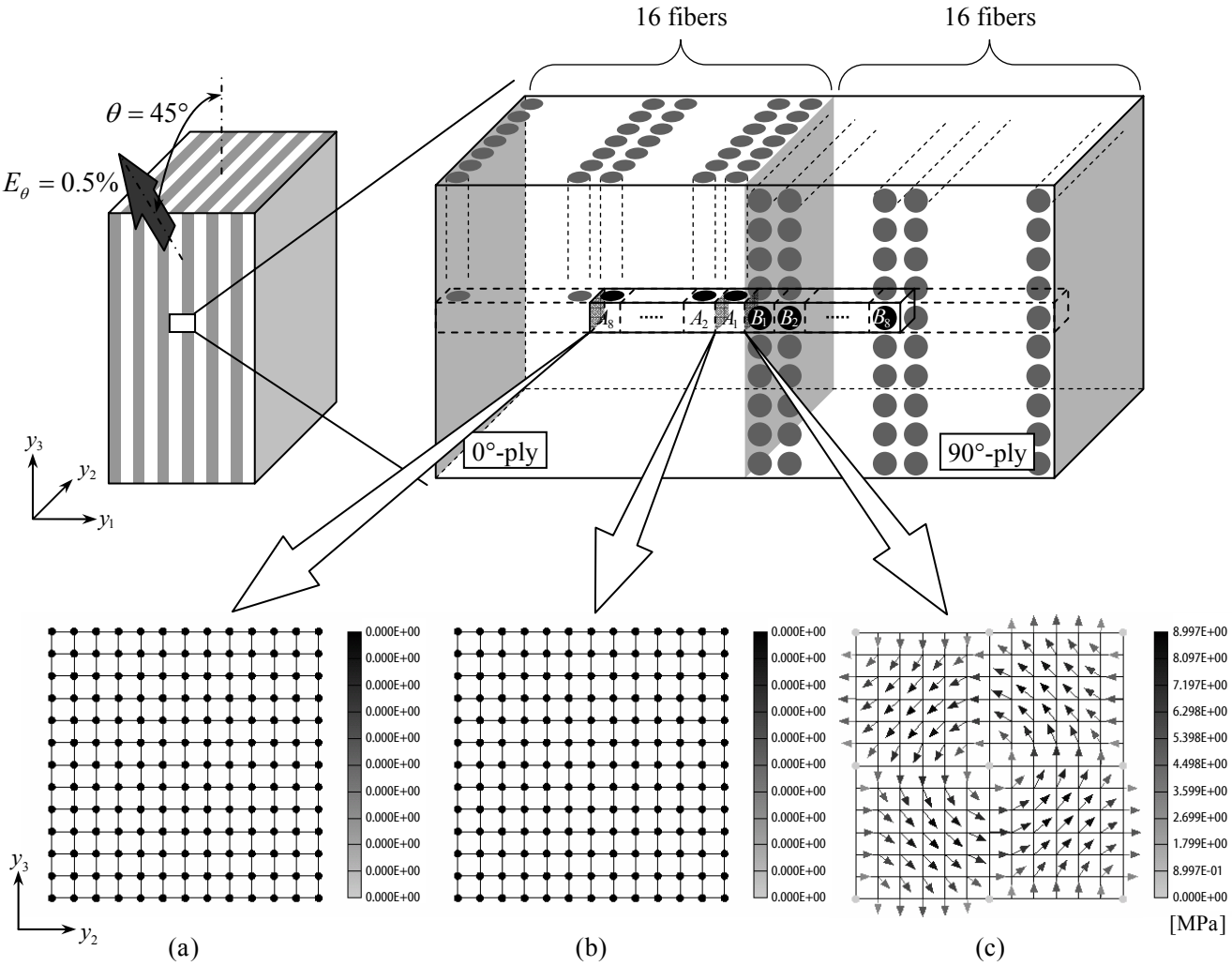

Fig. 4. Distributions of resultant shear stress $[(\sigma_{12})^2 + (\sigma_{13})^2]^{1/2}$ at (a) midsection of 0°-ply (left lateral facet of A_8), (b) vicinity of interlaminar plane (interface between A_1 and A_2), (c) interlaminar plane (interface between A_1 and B_1) at $E_\theta = 0.5\%$ ($\theta = 45°$).

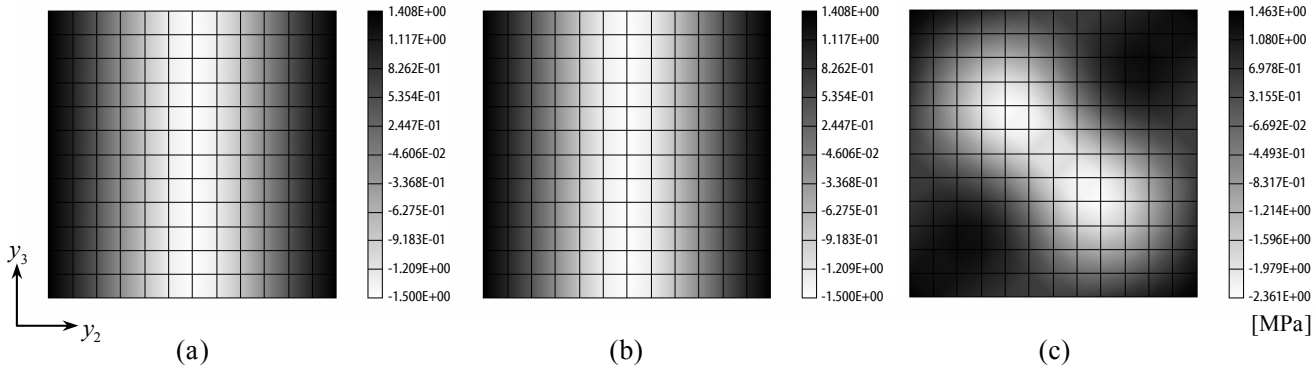

Fig. 5. Distributions of out-of-plane normal stress σ_{11} at (a) midsection of 0°-ply (left lateral facet of A_8), (b) vicinity of interlaminar plane (interface between A_1 and A_2), (c) interlaminar plane (interface between A_1 and B_1) at $E_\theta = 0.5\%$ ($\theta = 45°$).

Acknowledgement

The support in part by the Ministry of Education, Culture, Sports, Science and Technology, Japan under a Grant-in-Aid for Young Scientists (B) (No. 18760075) is acknowledged.

References

[1] Pagano N.J. and Rybicki E.F. “On the significance of effective modulus solutions for fibrous composites”. *Journal of Composite Materials*, Vol. 8, pp 214-228, 1974.

[2] Raghavan P., Moorthy S., Ghosh S. and Pagano N.J. “Revisiting the composite laminate problem with an adaptive multi-level computational model”. *Composites Science and Technology*, Vol. 61, pp 1017-1040, 2001.

[3] Ghosh, S., Lee, K., Raghavan, P., 2001. A multi-level computational model for multi-scale damage analysis in composite and porous materials. International Journal of Solids and Structures 38, 2335-2385.

[4] Raghavan, P., Ghosh, S., 2004. Concurrent multi-scale analysis of elastic composites by a multi-level computational model. Computer Methods in Applied Mechanics and Engineering 193, 497-538.

[5] Ghosh, S., Mukhopadhyay, S.N., 1993. A material based finite element analysis of heterogeneous media involving Dirichlet tessellations. Computer Methods in Applied Mechanics and Engineering 104, 211-247.

[6] Moorthy, S., Ghosh, S., 2000. Adaptivity and convergence in the Voronoi cell finite element model for analyzing heterogeneous materials. Computer Methods in Applied Mechanics and Engineering 185, 37-74.

[7] Matsuda, T., Ohno, N., Tanaka, H., Shimizu, T., 2002. Homogenized in-plane elastic-viscoplastic behavior of long fiber-reinforced laminates. JSME International Journal, Series A 45, 538-544.

[8] Matsuda, T., Ohno, N., Tanaka, H., Shimizu, T., 2003. Effects of fiber distribution on elastic-viscoplastic behavior of long fiber-reinforced laminates. International Journal of Mechanical Sciences 45, 1583-1598.

[9] Wu, X., Ohno, N., 1999. A homogenization theory for time-dependent nonlinear composites with periodic internal structures. International Journal of Solids and Structures 36, 4991-5012.

[10] Ohno, N., Wu, X., Matsuda, T., 2000. Homogenized properties of elastic-viscoplastic composites with periodic internal structures. International Journal of Mechanical Sciences 42, 1519-1536.

[11] Bensoussan, A., Lions, J.L., Papanicolaou, G., 1978. Asymptotic Analysis for Periodic Structures. North-Holland Publishing Company, Amsterdam.

[12] Sanchez-Palencia, E., 1980. Non-Homogeneous Media and Vibration Theory, Lecture Notes in Physics, No. 127. Springer-Verlag, Berlin.

[13] Bakhvalov, N., Panasenko, G., 1984. Homogenisation: Averaging Processes in Periodic Media. Kluwer Academic Publishers, Dordrecht.

[14] Ohno, N., Matsuda, T., Wu, X., 2001. A homogenization theory for elastic-viscoplastic composites with point symmetry of internal distributions. International Journal of Solids and Structures 38, 2867-2878.

[15] Zienkiewicz, O.C., Taylor, R.L., 2000. The Finite Element Method, 5th Edition. Butterworth-Heinemann, Oxford.

[16] Okumura, D., Ohno, N., Noguchi, H., 2004. Elastoplastic microscopic bifurcation and post-bifurcation behavior of periodic cellular solids. Journal of the Mechanics and Physics of Solids 52, 641-666.

[17] Ohno, N., Okumura, D., Noguchi, H., 2002. Microscopic symmetric bifurcation condition of cellular solids based on a homogenization theory of finite deformation. Journal of the Mechanics and Physics of Solids 50, 1125-1153.